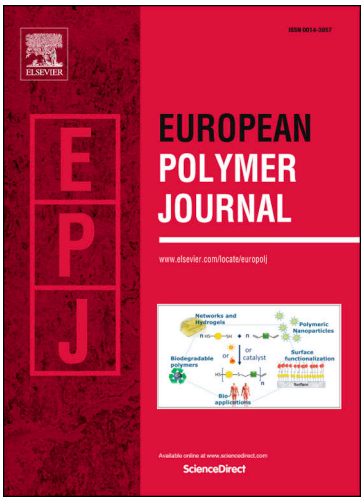

New side-chain liquid crystalline terpolymers with anhydrous conductivity: effect of azobenzene substitution on light response and charge transfer

Sakinah Mohd Alauddin, A. Ramadan Ibrahim, Nurul Fadhilah Kamalul Aripin, Thamil Selvi Velayutham, Osama K. Abou-Zied, Alfonso Martinez-Felipe

PII: S0014-3057(20)31963-7
DOI: https://doi.org/10.1016/j.eurpolymj.2020.110246
Reference: EPJ 110246

To appear in: *European Polymer Journal*

Received Date: 27 September 2020
Revised Date: 10 December 2020
Accepted Date: 23 December 2020

Please cite this article as: Mohd Alauddin, S., Ramadan Ibrahim, A., Fadhilah Kamalul Aripin, N., Selvi Velayutham, T., Abou-Zied, O.K., Martinez-Felipe, A., New side-chain liquid crystalline terpolymers with anhydrous conductivity: effect of azobenzene substitution on light response and charge transfer, *European Polymer Journal* (2020), doi: https://doi.org/10.1016/j.eurpolymj.2020.110246

New side-chain liquid crystalline terpolymers with anhydrous conductivity: effect of azobenzene substitution on light response and charge transfer.

Sakinah Mohd Alauddin [1,2], A. Ramadan Ibrahim[3], Nurul Fadhilah Kamalul Aripin [1,2,*], Thamil Selvi Velayutham[2,4], Osama K. Abou-Zied[3] and Alfonso Martinez-Felipe [5,*]

[1] Faculty of Chemical Engineering, Universiti Teknologi MARA, 40450 Shah Alam, Selangor Darul Ehsan, Malaysia. sakinah3676@uitm.edu.my; fadhilah9413@uitm.edu.my.

[2] Fundamental and Frontier Sciences in Nanostructure Self-Assembly Center, Department of Chemistry, Faculty of Science, University of Malaya, 50603 Kuala Lumpur, Malaysia.

[3] Department of Chemistry, Faculty of Science, Sultan Qaboos University, P.O. Box 36, Postal Code 123, Muscat, Sultanate of Oman. a.ibrahim@squ.edu.om; abouzied@squ.edu.om.

[4] Low Dimensional Material Research Center, Department of Physics, Faculty of Science, University of Malaya, 50603 Kuala Lumpur, Malaysia. t_selvi@um.edu.my

[5] Chemical and Materials Engineering Research Group, School of Engineering, University of Aberdeen, King's College, Old Aberdeen AB24 3UE, UK. a.martinez-felipe@abdn.ac.uk.

***** Correspondence: a.martinez-felipe@abdn.ac.uk and fadhilah9413@uitm.edu.my.

Abstract

We have prepared and characterised a series of side-chain liquid crystalline homopolymers and terpolymers containing different azobenzene derivatives (*R*AzB), sulfonic groups (2-acrylamido-2-methyl-1-propanesulfonic acid, AMPS), and methyl(methacrylate) groups (MMA), as monomeric units. We have evaluated the effect of different *para*-substitutes of 6-(4-azobenzene -4'-oxy)hexyl methacrylate, at the side chains, OCH_3, NO_2 and H, on the phase behaviour and conductivity of the new polymers. The copolymers can form smectic and nematic phases, depending on their composition, and have light responsiveness, conferred by the azobenzene chromophores. The terpolymer with methoxy terminations, MeOAzB/AMPS/MMA, exhibits the highest conductivity values of the series ($10^{-2}/10^{-3}$ $S \cdot cm^{-1}$ range) through liquid crystalline phases and with signs of decoupling from polymeric segmental motions. These materials are promising candidates to develop new light-responsive polymeric electrolytes for electrochemical conversion devices in which ionic conductivity under anhydrous conditions can be controlled by their nanostructure.

Keywords: side-chain liquid crystal polymers; ionic conductivity; azobenzene; energy conversion; polymer electrolytes

1. Introduction

Universal access to sustainable and reliable energy is a global challenge as worldwide energy demand is expected to rise rapidly by 1.3% by 2040 [1], and the development of alternative and more efficient technologies will help achieve decarbonisation through diversification of energy sources. Renewable sources are expected to increase during recovery from the Covid-19 outbreak, due to low operating costs, preferential access to power systems and diversity of existing projects. [2] The design of advanced electrolytes is crucial to achieve more efficient technologies for energy harvesting, storage and conversion, and to ultimately offset the variability of renewable energy sources by improving electrochemical processes. [3] In the preparation of novel electrolytes, manipulation of the nanoscale *via* external stimuli offers new and fascinating frontiers in technological applications, as a mechanism to control the transport of mass, charge and energy in integrated systems, which could be operated remotely. Liquid crystals form intermediate states of order between crystalline solids and isotropic liquids, [4] and the resulting combination of molecular mobility and long-range order can not only promote high ionic conductivity[5, 6], but also trigger different mechanism of ionic transport[7]. Some examples include 3D structures obtained with Zwitterions,[8] or cylindrical aggregates containing poly(vinyl catechol)s and polystyrenes doped with silver nanoparticles [9], among many others.[10]

The application of light is particularly appealing to exert spatial control on molecular order of nanostructured materials, *via* valence and E/Z isomerisations, cycloadditions or tautomerisations,[11-14], resulting in chromophoric sensors and actuators that can trigger electrochemical processes. Azobenzenes have been widely used as components in light-responsive liquid crystals, due to their molecular anisotropy that can be switched by the application of UV and visible light. [15] More specifically, the azobenzene *trans* isomer has a linear molecular geometry that can assist the formation of mesophases by promoting anisotropic interactions. Irradiation with UV light at ~365 nm triggers *trans*-to-*cis* photoisomerisation of the azobenzene group, and the resulting *cis* isomer has a curved geometry with a net dipole moment in the $\vec{\mu} \sim 3\ D$ range [16]. *Cis*-to-*trans* relaxation takes place spontaneously by thermal activation, or by the application of light at longer wavelengths (~420 nm). The change in molecular geometry can disrupt the liquid crystalline order in azo-containing materials used as electrolytes, ultimately controlling their transport properties. [17, 18]

Liquid crystalline electrolytes have great potential to yield anhydrous conductivity in solvent-free electrolytes,[19] *via* anisotropic ion hopping assisted by hydrogen-bonding between neighbouring polar groups.[20-24] Recently, we have investigated a series of side-chain liquid

crystalline polymers, SCLCPs, that self-assemble into ion-rich domains in the absence of solvents [25-27]. SCLCPs can show promising electrolyte performance, with conductivity values within the 10^{-3} S cm^{-1} range, yielding simultaneous ionic conductivity and liquid crystalline behaviour.[21, 25-33] One remaining challenge is to decouple the motions of the mesogenic groups in the side chains from the rigidity of the polymer backbone, in order to preserve both local molecular mobility and charge conductivity at sufficiently low temperatures. In this work, we evaluate the effect of composition on the molecular structure and electrolyte response of a new series of SCLCPs containing azobenzenes, with the general structure shown in **Fig. 1**.

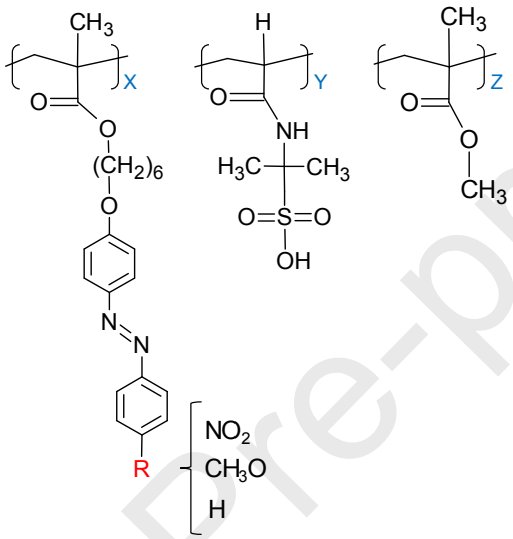

Figure 1. Chemical structure of the *R*AzB/AMPS/MMA terpolymers containing different terminal groups (*R* = NO_2, CH_3O, H) at the mesogenic chains. *X*, *Y* and *Z*, represent molar percentages in the terpolymers (% molar), respectively, and the corresponding homopolymers (*R*AzB, with X=100, Y=Z=0) were also studied.

We have copolymerised derivatives of the 6-(4-azobenzene -4'-oxy)hexyl methacrylate, as mesogenic monomers in the side-chains (*R*AzB), together with the commercial 2-acrylamido-2-methyl-1-propanesulfonic acid (AMPS), as the polar monomeric unit. The inclusion of methacrylate units (MMA), on the other hand, can regulate the interactions involving the conducting and mesogenic components in the resulting terpolymers, and can facilitate the formation of films.[25] We have explored the effect of electro-withdrawing and electro-donating groups on the polymers' response to light and charge mobility by including *para*-substituted azobenzenes with nitro (*R* = NO_2) and methoxy (*R* = CH_3O) groups, as terminal groups at the side chains. Additionally, we have also included non-substituted azobenzenes (*R* = H) as monomeric units. By using the six-methylene flexible spacers we expect to decouple the motions of the rigid azobenzene group respect to the polymer main chain[34], and to compare our results with previous findings on SCLCPs that contain longer methylene spacers.

2. Experimental procedure

Materials preparation

AMPS and MMA were commercially available from Sigma-Aldrich. MMA was purified by washing with sodium hydroxide and water, followed by drying with anhydrous magnesium sulphate; AMPS was used without further purification, and the azobenzene monomers (*R*AzB) were prepared by diazonium salt coupling of the respective aniline derivatives according to previous procedures [35-37]. Polymers were prepared by conventional free radical polymerisation under an inert atmosphere. For the synthesis of the terpolymers, equimolar amounts of the different monomers were added to the reaction vessel[27]. Further details of the synthetic procedure are provided in the Electronic Supplementary Information, ESI (**Fig. ESI1** to **ESI6**).

Characterisation Techniques

Nuclear magnetic resonance, ^{1}H-NMR, and Fourier-transform infrared spectroscopy, FT-IR, were used to assess the chemical structures of the monomers and polymers, and gel permeation/ size exclusion chromatography, GPC/SEC, was applied to determine number average molecular weights (Mn) and weight average (Mw) molecular weights, polydispersities (Mw/ Mn), and degrees of polymerisation (DP). The thermal stability of the polymers was assessed by thermogravimetric analysis, TGA. The formation of liquid crystalline phases was determined by differential scanning calorimetry, DSC, and polarised optical microscopy, POM, and their structures were evaluated by X-ray diffraction, XRD. Molecular lengths were estimated using ACD/ChemSketch software.

UV-visible absorption spectra of films cast on quartz substrates and $3.59 \cdot 10^{-5}$ M THF solutions were measured at room temperature using an HP 845x Diode Array spectrophotometer. The photoirradiation experiments were carried out by first heating the samples to 75^{o}C for 2 h (using a Peltier temperature controller), then irradiating for 10 min at 365 nm under a multiband UV lamp (Mineralight Lamp UVGL-55; 230 V and 6 W). Samples were then cooled down rapidly to 22^{o}C and kept in the dark and their absorbance was obtained at various time intervals until the spectra recovered their original shape (by thermal relaxation). Ionic conductivity was measured by impedance spectroscopy, at isothermal steps when cooling from the isotropic phase, and additional dielectric measurements were carried out under similar conditions.

Further information and details on the procedures, equipment and conditions used during materials characterisation, are included as Electronic Supplementary Information.

3. Results and discussion

3.1 Polymers preparation

The names of the homopolymers and terpolymers synthesised in this work, as well as their relevant compositional features, are summarised in **Table 1**. The chemical structures were confirmed by ^{1}H-NMR and FT-IR, see **Fig. ESI7** to **ESI11**, and molar fractions of the *R*AzB/AMPS/MMA terpolymers were estimated by calculating the relative integrals of the 7-8 ppm ^{1}H-NMR signals (phenyl azobenzene protons of *R*AzB, 8H), the ~2.7 ppm singlet (methylene groups adjacent to the sulfonic acid groups in AMPS, 2H) and the singlet at ~3.6 ppm (methyl groups of MMA, 3H), see **Fig. ESI10** as an example. All polymers show moderate to low polydispersity ratios (Mw/Mn between 1 and 2.3), and the dispersity of the chains' distribution increases upon copolymerisation, **Fig. ESI12**. This fact was somehow expected, due to the different reactivity rates of the three monomers involved [38-40], but we note that our Mw/Mn values are smaller than for other copolymers with comparable sulfonic groups concentrations. [27, 41-44] Even though convectional radical polymerisation techniques pose some limitations to control polydispersity, the present one-pot preparation method is simple and avoids further and costly synthetic stages. We cannot rule out, however, the formation of tapered chains initiated by polymerisation of similar units, to which other groups attach, following blocky distributions.[27] The terpolymers show high molecular weights, in the 67 – 82 kg mol^{-1} range, which can be beneficial for the preparation of self-standing films and their application as electrolytes.

Table 1. Sample names of the *R*AzB/AMPS/MMA terpolymers and the homopolymers, *R*AzB, and experimentally assessed molar percentages of azobenzene (*R*AzB, X), AMPS (Y) and MMA (Z), monomeric units. Number average molecular weight and weight average molecular weight, Mn and Mw, respectively, polydispersities, Mw/Mn, and number average degree of polymerization, DP.

Sample	Composition X/Y/Z Molar %	Mn g·mol^{-1}	Mw g·mol^{-1}	Mw/Mn	DP
MeOAzB	100/0/0	15570	22507	1.5	42
MeOAzB/AMPS/MMA	40/25/35	36168	67158	1.9	125
NO2AzB	100/0/0	10520	18958	1.8	26
NO2AzB/AMPS/MMA	21/34/45	36012	81135	2.3	153
HAzB	100/0/0	3787	4763	1.3	10
HAzB/AMPS/MMA	21/44/35	43164	80360	1.9	189

Fig. 2(a) and **2(b)** show the thermogravimetric (TG) and derivative thermogravimetric (DTG) curves of the polymers, respectively, which are in excellent agreement with thermal

degradation profiles found in similar azobenzene-containing copolymers [25, 27], and the main associated parameters are summarised in **Table ESI1**. Thermal degradation initiates with one weight-loss process starting around 300°C, which can be attributed to decomposition of lateral units in the side chains, followed by further degradation at higher temperatures (~ 400°C), associated with breakage of the main polymer chains [45, 46]. The presence of polar groups (NO_2, AMPS and $COOCH_3$) seems to increase the liability of the side chains in the polymers, by shifting the initial process towards lower temperatures (T< 300ºC). We note that temperatures corresponding to 2% weight losses are above $T_{2\%}$ >250ºC, which confirms that these polymers could be used at nominal operational conditions of proton exchange membrane fuel cells.

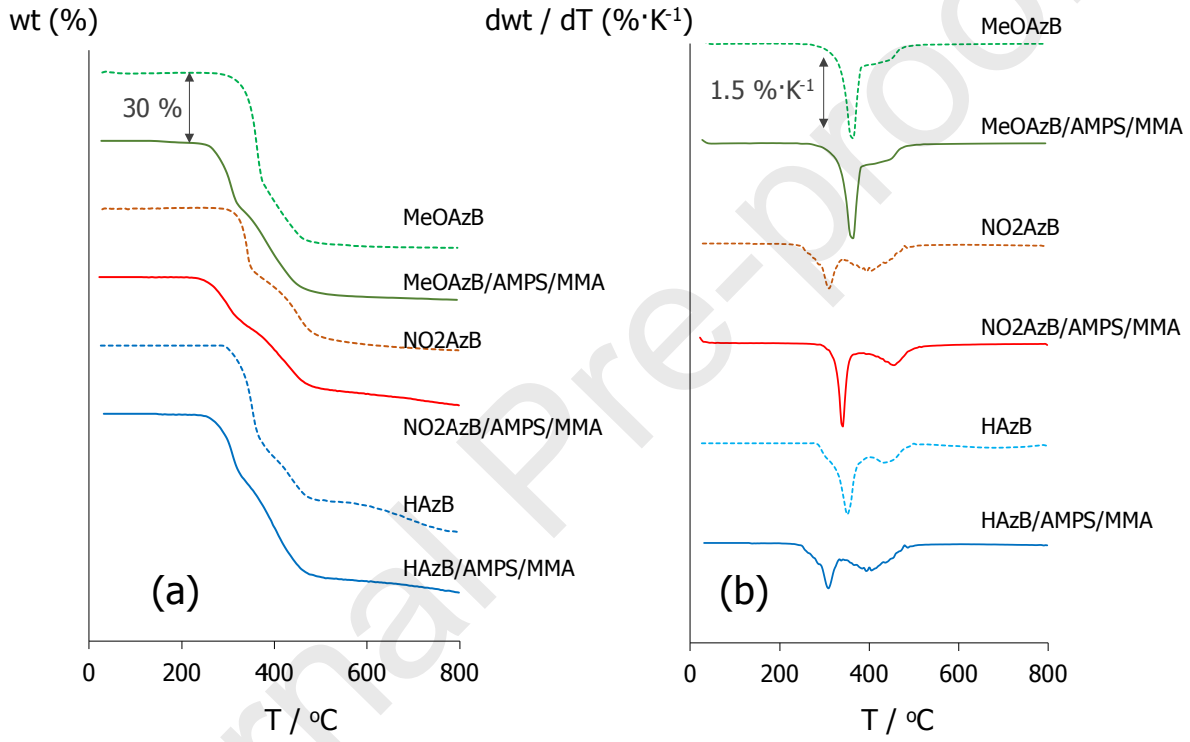

Figure 2. Thermogravimetric (TG) and derivative thermogravimetric (DTG) curves of the *R*AzB homopolymers and *R*AzB/AMPS/MMA terpolymers, showing weight (wt) percentage and its derivative over temperature (dwt/dT). Curves have been shifted arbitrarily along the Y-axes.

3.2 Phase behaviour and structure

The phase behaviour and structure of the homopolymers and terpolymers were studied by differential scanning calorimetry, DSC, and X-ray diffraction, XRD, and the appearance of liquid crystalline phases was further assessed by the observance of birefringent areas under the polarised optical microscope, POM, which flickered upon application of pressure. Like

other liquid crystalline polymers, the POM textures were not well-defined, and were not helpful for phase assignation, see **Fig. ESI13**, except for MeOAzB, which shows schlieren and focal conic fan textures, characteristic of nematic and smectic phases, respectively. **Fig. 3** shows the DSC thermograms of the homopolymers and terpolymers, and the corresponding thermal parameters are summarised in **Table 2**.

MeOAzB shows in **Fig. 3** a pseudo-second order transition at low temperatures, associated with its glass transition (T_g ~ 74°C), followed on heating by two first-order transitions: smectic to nematic, T_{SmAN} = 94°C, and nematic to isotropic, T_{NI}=134°C. These results are in excellent agreement with previous reports on comb-like poly(methyl methacrylate)s *para*-substituted with methoxy groups. [47, 48] The formation of smectic phases is consistent with the MeOAzB X-ray diffractogram, obtained at room temperature when cooling from the isotropic phase, see **Fig. 4**. The curve shows two sharp reflections related to spacings of the smectic periodicity: at d_1 ~15.0 Å, and the corresponding higher order reflections, at d'_1 ~7.3 Å and d''_1 ~4.5 Å, which may correspond to the d ~30.0 Å smectic distance, see **Table 3**. The XRD pattern of the NO2AzB homopolymer also has signs of smectic phases, and shows a diffraction at small angles at d_0 ~25.2 Å, together with another diffraction at d_1 ~ 13.6 Å, see also **Fig. 4**. The broad first order transition observed in the DSC thermogram of this homopolymer in **Fig. 3** has a large associated enthalpy ($\Delta S_{LCI}/R$ = 0.40) and could indicate a merged isotropic to nematic and nematic to smectic transition, taking place at higher temperatures than MeOAzB, T_{LCI}=150°C.[47, 48] HAzB, on the other hand, does not show liquid crystalline phases, according to our DSC and XRD results.

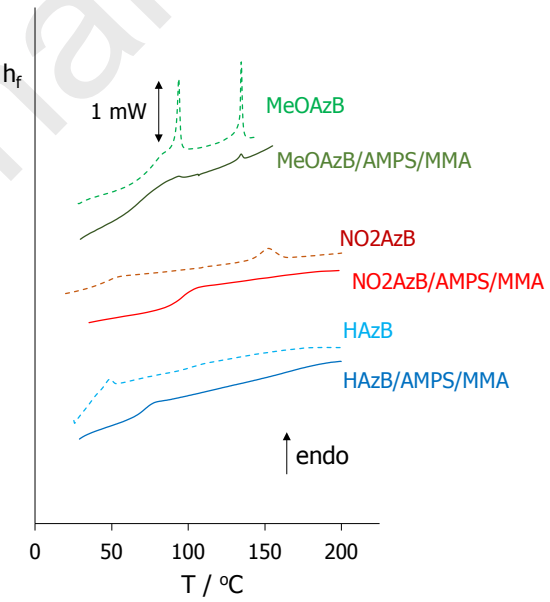

Figure 3. Differential scanning calorimetry, DSC, thermograms obtained in the second heating scans of the homopolymers (dotted lines) and terpolymers (solid lines). Curves have been shifted arbitrarily along the Y-axis (h_f, heat flow).

Table 2. Glass transitions, T_g, transition temperatures, T_i, and associated enthalpies, ΔH_i, and reduced entropies, $\Delta S_i/R$, calculated from the DSC thermograms of the homopolymers and terpolymers, obtained during their second heating scans. LC, liquid crystal; Sm, smectic; N, nematic; I, isotropic; R is the gas constant.

Sample	T_g (°C)	T_{SmN} / °C ΔH_{SmN} / J·g^{-1} ΔS_{SmN}/ R	T_{LCI} / °C ΔH_{LCI} / J·g^{-1} ΔS_{LCI}/R
MeOAzB	79.0	94 4.27 0.55	134 [a] 2.9 [a] 0.34 [a]
MeOAzB/AMPS/MMA	74.0	*	135 [a] 0.21 [a] 0.04 [a]
NO2AzB	58.0	-	150 [b] 3.38 [b] 0.40 [b]
NO2AzB/AMPS/MMA	97.6	-	-
HazB	46.5	-	-
HAzB/AMPS/MMA	73.6	-	-

* Weak transition, merged with T_g.
[a] Nematic to isotropic transition.
[b] Liquid crystal to isotropic transition.

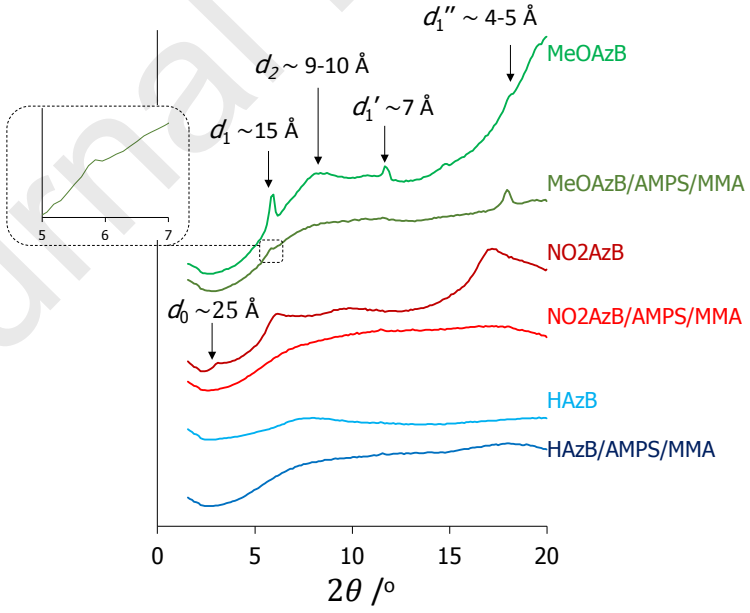

Figure 4. XRD scatterings obtained at room temperature, 25°C, by cooling the polymers from their isotropic or liquid crystalline phases, highlighting relevant reflections d_i. Y-axis corresponds to the diffractogram intensity, a.u., and curves have been shifted arbitrarily along this axis.

Table 3. Summary of the main reflections obtained from the X-ray diffractograms of the polymers, measured at room temperature on cooling from the isotropic and liquid crystalline phases (T=25°C).

Sample	d_i / Å				
	d_0	d_1	d_1'	d_2	d_1''
MeOAzB		15.0	7.3	9.7	4.8
MeOAzB/AMPS/MMA		14.2		9.8 [b]	4.8
NO2AzB	25.2	13.6		8.6	5.1
NO2AzB/AMPS/MMA		7.8[w]			4.8 [b, w]
HAzB				11.0 [b]	
HAzB/AMPS/MMA					4.8 [b]

[b] Broad signal.

[w] Weak signal.

The liquid crystalline phases in NO2AzB and MeOAzB are facilitated by the stacked structure of the *trans*-azobenzene units at the side chains, whilst the flexible linkages allow to decouple, at least to some extent, the mobility of the rod-like group from the polymeric backbone. [34, 36, 49] The length of the spacers, n=6, is enough for the $(CH_2)_6$ and the azobenzenes to micro-segregate into non-polar and polar domains, and the *para*-substitution with CH_3O and NO_2 terminal groups stabilises core-to-core lateral interactions, by extending the electronic density of the azobenzene groups. We believe that NO2AzB and MeOAzB may form fully interleaved SmA_1 phases, with azobenzene groups arranged in an antiparallel fashion. Whilst this later model is energetically unfavourable due to some degree of mixing between methylene chains and the azobenzenes, it might optimise packing efficiency within the smectic layers.[41] This interleaved molecular distribution can be assigned to the d_1 diffraction in **Table 3**, and the absence of a higher order diffraction could be then explained by quasi-symmetrical distributions of the electronic density about the mid-point of the smectic layers. [47, 50] The actual phase structure of the homopolymers could correspond to an incommensurate smectic phase with a combination of different arrangements. The sharp signals in **Fig. 4** overlap with broad reflections, attributed to the length of the *trans* azobenzene isomer, d_2 ~10 Å, and to the periodicity along the polymer backbone, d ~5 Å.

In the terpolymers, the non-mesogenic AMPS and MMA monomeric units may dilute the interactions between the azobenzenes [5, 34]. As a result, NO2AzB/AMPS/MMA and HAzB/AMPS/MMA do not show evidence of liquid crystalline behaviour, and only their glass transitions are visible in their respective DSC thermograms, see **Fig. 3**. Alternatively, MeOAzB/AMPS/MMA shows thermal transitions at comparable temperatures to those of the MeOAzB homopolymer, but with much weaker intensities, hence suggesting the formation of

nematic and smectic phases. This fact can be explained, at least in part, by the higher concentration of azobenzene units in this terpolymer, [MeOAzB] ~40%, compared to those in NO2AzB/AMPS/MMA or HAzB/AMPS/MMA, [*R*AzB] ~20%, see **Table 1**. This result is in agreement with our previous observations on statistical and block copolymers, which indicated that a minimum of around 30% molar concentration of mesogenic groups is necessary to maintain liquid crystalline behaviour.[25, 27] The MeOAzB/AMPS/MMA diffractogram in **Fig. 4** further supports the formation of smectic phases in this polymer. The almost equal distance for MeOAzB and MeOAzB/AMPS/MMA suggests the formation of a separated smectic phase with MeOAzB units, coexisting with disordered AMPS regions in the terpolymer.

3.3 UV light-response

Fig. 5(a) and **5(b)** show the UV-visible absorption spectra of the polymers obtained in THF solution and on quartz films, respectively, measured at room temperature. The lowest-energy UV absorption band falls in the 340 – 380 nm range, and is due to a $\pi^* \leftarrow \pi$ transition in the *trans*-azobenzene chromophore. A very weak absorption band is also visible at longer wavelength, 420 - 450 nm, and is assigned to a weak $\pi^* \leftarrow n$ transition in *cis*-azobenzenes.[51]

In solution, HAzB shows a maximum at 348 nm, and *para*-substitution in the azobenzene molecule shifts the absorbance towards longer wavelengths, with maxima at 357 nm (CH_3O) and 375 nm (NO_2), see **Fig 5(a)**. These bathochromic shifts are consequences of the substitution of the azobenzene groups by electron-donating (CH_3O) and electron-withdrawing (NO_2) groups. It is clear from the spectra that both the homo- and terpolymers have the same absorption pattern in each case. The large red shift in the case of the NO_2-substituted polymers suggests that their electronic transition involves a migration of electron density from the donor group (polymer chain) to the acceptor group (NO_2), stabilising the π^* excited state. This intramolecular charge transfer gives rise to more accessible states that produce the observed wide, structureless peak. The CH_3O- ended compounds, on the other hand, show structured absorbance that includes well-defined peaks, possibly arising from different vibronic transitions involving the ground and excited states. The exact spectral position matching MeOAzB and its terpolymer, MeOAzB/AMPS/MMA, implies minimal or no charge transfer from the rest of the polymer components to the chromophore in solution. This observation can be explained by the stronger electron donating ability of the terminal methoxy group, compared to the polymer backbone and the rest of functional groups in the terpolymer. It is worth mentioning that the structured absorbance peak in the CH_3O-

substituted polymers is similar to that reported for the azobenzene molecule[52], confirming a local excitation in the chromophore molecule.

In film, all polymers show broader $\pi^* \leftarrow \pi$ absorption spectra than in solution, with the CH_3O-substituted polymers still maintaining structured absorbance, **Fig. 5(b)**. The broadness in the spectra could be due to the formation of H-aggregates (at lower wavelengths, head-to-head/parallel arrangements), and J-aggregates (at higher wavelengths, corresponding to head-to-tail arrangements), however, some potential scattering effects cannot be totally ruled out. [18, 51] It is noticeable that absorption of the *cis*-isomer is enhanced in HAzB and the corresponding terpolymer, HAzB/AMPS/MMA, whilst it is difficult to determine such effect in the MeOAzB and NO2AzB polymers, due to the broadness of the signal overlapping the 420–450 nm region.

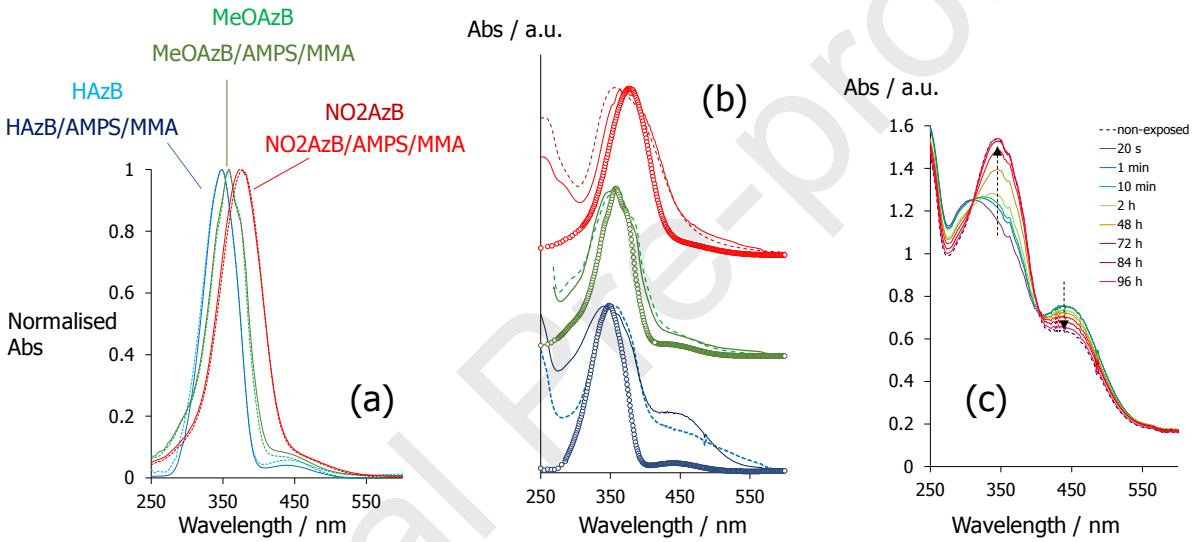

Figure 5. UV-visible spectra of the homopolymers and terpolymers (UV-vis absorbance, Abs) measured at room temperature, obtained for: (a) 3.73 x 10^{-5} M THF solutions; (b) films cast on quartz substrates; the corresponding spectra in solution (for homopolymers) are shown for comparison as circles; (c) photoisomerisation of HAzB/AMPS/MMA; dotted line corresponds to the original spectrum of the HAzB/AMPS/MMA film prior to UV exposure (non-exposed) and after heating to 75°C for two hours, and dotted arrows indicate the *cis*-to-*trans* thermal relaxation with time, *t*, after exposure, while keeping the samples in the dark after immediate cooling to 22°C.

Upon irradiation with UV light at 365 nm, the $\pi\pi^*$ band decreases rapidly in intensity for all the samples under study, with a concomitant intensity increase in the 420–450 nm region. This observation is due to *trans*-to-*cis* isomerisation of the azobenzene groups. **Fig. 5(c)** illustrates this effect for the HAzB/AMPS/MMA film. [53] When the sample is kept in the dark, the intensity of the $\pi\pi^*$ band increases with time and recovers after 96 hours to the original absorption pattern due to the thermally activated *cis*-to-*trans* relaxation. We have observed

comparable photoisomerisation behaviour in the rest of samples under study, and in the case of MeOAzB, the recovery of the UV-vis absorption values measured on a film at 100ºC confirms that the liquid crystal phase is reformed after illumination, see **Fig. ESI14**. Considering that photoisomerisation involves kinetics phenomena that depend on several variables (light intensity and frequency, time, temperature), a more detailed study on irradiation and recovery of these polymers will be the subject of further work.

3.4 Conductivity and charge transport

The conductivity of the polymers was studied by impedance spectroscopy, in frequency sweeps at different isothermal steps when cooling from the isotropic phases, as described in the ESI. More specifically, we measured the complex dielectric permittivity, $\varepsilon^* = \varepsilon' - i\varepsilon''$, which was then transformed into complex impedance, Z^*, and conductivity, σ^*, using: [54]

$$Z^* = Z' + iZ'' = \frac{1}{i\omega C_0 \varepsilon^*} \qquad \text{Eq. 1}$$

and,

$$\sigma^* = i\,\omega\varepsilon_0\varepsilon^* \qquad \text{Eq. 2}$$

where $i = \sqrt{-1}$ is the imaginary unit, ω is the angular frequency in $\mathrm{rad} \cdot \mathrm{s}^{-1}$, C_0 is the cell capacitance and ε_0 is the permittivity in the vacuum, $8.854x10^{-12} F\,m^{-1}$.

Typical impedance responses of the polymers consisted of supressed semicircles (high frequencies) followed by a straight line (low frequencies), see **Fig. ESI15**, and direct current (DC) conductivity, σ_{dc}, corresponded to the Z' value at the spike between these trends in the Nyquist plots (Z'' *vs* Z'), and was obtained at each temperature from the plateaus in the isothermal log(σ') *vs* log(*f*) plots in **Fig. 6**. Whilst homopolymers show low conductivities (in the 10^{-8} S cm^{-1} range) due to the absence of polarisable groups, the introduction of sulfonic groups promotes ionic conductivity through the *R*AzB/AMPS/MMA terpolymers. Indeed, the three terpolymers display visible DC conductivity across broad temperature ranges, and we show the corresponding σ_{dc} Arrhenius plots in **Fig. 7**.

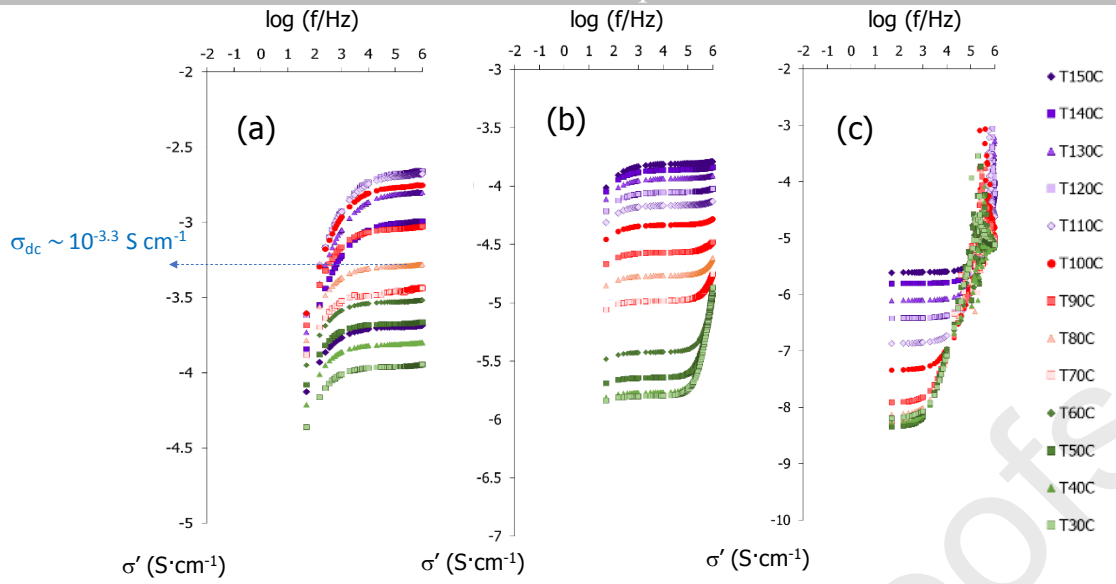

Figure 6. Double logarithmic plots of the real component of the complex conductivity, σ', measured as a function of the frequency, log(σ') *vs* log(*f*), in isothermal steps (°C) on cooling from the isotropic phases for: (a) MeOAzB/AMPS/MMA; (b) HAzB/AMPS/MMA and (c) NO2AzB/AMPS/MMA. Estimation of DC conductivity, σ_{dc}, at T=80°C for MeOAzB/AMPS/MMA.

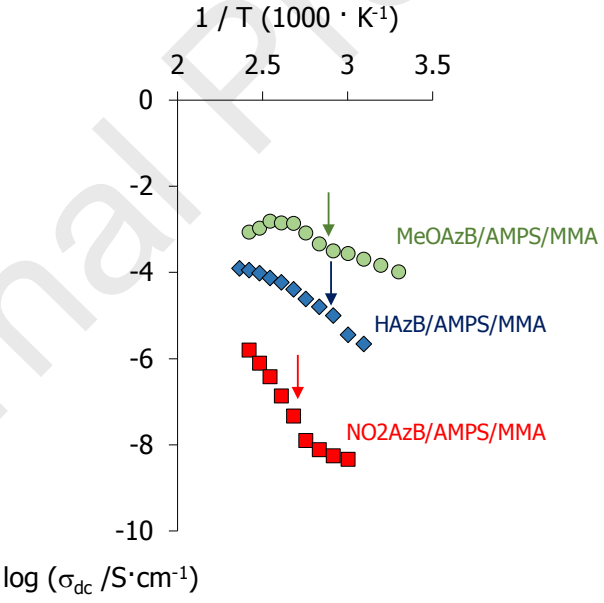

Figure 7. Arrhenius plots (in $\log_{10}$ scale) of the DC conductivity, σ_{dc}, calculated for the *R*AzB/AMPS/MMA terpolymers. Arrows indicate their glass transitions, T_g.

Conductivity increases with temperature, particularly above the polymers' glass transitions, due to the largest free volume that is available after segmental motions of the polymer backbone are thermally activated.[55] MeOAzB/AMPS/MMA shows the highest conductivities in the series, reaching the maximum at the liquid crystal range ($\sigma_{dc} \sim 10^{-2.9}$ S cm^{-1}, measured

at 110ºC). We note that, to the best of our knowledge, these σ_{dc} values are within the highest levels of conductivity reported for non-doped liquid crystalline polymers, [21, 25-33] and this fact is particularly remarkable considering the low concentration of polarisable AMPS groups in this terpolymer ([AMPS] ~ 25% molar %, see **Table 1**). Even though our microscopic observations do not allow for an unequivocal phase assignation, see again **Fig. ESI13**, the calorimetric thermograms of MeOAzB/AMPS/MMA in **Fig. 3** suggest the formation of a nematic phase, and the relatively low viscosity of this mesophase could contribute to the highest σ_{dc} values observed in **Fig. 7**.[21] On further cooling MeOAzB/AMPS/MMA, the drop in σ_{dc} could be explained by the formation of a smectic phase with higher viscosity, with ionic motions potentially taking place in the acid-rich domains discussed earlier.

We have studied the thermal activation of conductivity from the Arrhenius plots in **Fig. 7**, and at high temperatures, the thermal dependence of the ionic conductivity (σ_{dc}) can be described by the Vogel-Fulcher-Tamman equation,[56]

$$\sigma_{dc} = \frac{A}{\sqrt{T}} \exp\left(\frac{-B}{T - T_o}\right) \qquad \text{Eq. 3}$$

where A is proportional to the concentration of carrier ions, *B* is the pseudo-activation energy for ion conduction, and T_o is the ideal glass transition temperature. Direct conductivity at low temperatures follows a linear behaviour, and the activation energies, E_a, can be then calculated using the Arrhenius equation,

$$\sigma_{dc} = \sigma_0 \exp\left(\frac{E_a}{R}\frac{1}{T}\right) \qquad \text{Eq. 4}$$

where *R* is the gas constant, 8.31 J mol^{-1} K^{-1}, *T* is the absolute temperature, and σ_0 is a pre-exponential term.

Table 4 shows the parameters in **Eq. 3** and **Eq. 4**, calculated for some of the terpolymers under study and other related materials. The low activation energy (E_a ~26 kJ mol^{-1}) and apparent activation energy (B = 299 K) associated with the conductivity processes through MeOAzB/AMPS/MMA suggest that ion mobility can be decoupled from the segmental motions of the polymer main chain in this terpolymer. More specifically, whilst the high temperature process (80 / 120ºC) can be associated with the onset of the glass transition (T_g=74ºC), the linear process at low temperatures (30 / 80ºC) can be linked to the vitrification of the smectic domains. These results contrast with larger E_a and *B* values reported for NO2AZB/AMPS/MMA in **Table 4**, which could reflect on its high glass transition, T_g ~98ºC, and would result in the lower σ_{dc} values observed for this terpolymer in **Fig. 7**. Hence, the higher rigidity of NO2AzB/AMPS/MMA in the series results in lower ionic mobility, probably associated to lower free volume available. The difference in the activation energies of

MeOAzB/AMPS/MMA and HAzB/AMPS/MMA, on the other hand, could be then explained by the formation of smectic glasses by the former, where the acid groups responsible for conductivity are separated from the mesogenic azobenzene groups. We note that, unfortunately, only one of our terpolymers showed liquid crystal behaviour, and a comparison of the conductivity performance cannot be argued in terms of terminal groups between liquid crystalline copolymers. It is worth noting, however, that the sole liquid crystalline copolymer in the series, MeOAzB/AMPS/MMA, has shown the most promising conductivity values.

Table 4. Kinetic parameters of the conductivity processes in the terpolymers, including values obtained for reference comb-shaped poly(methacrylate)s (see structures in **Fig. ESI16**).

Sample	Conductivity					
	Low temperature		High temperature			
	E_a / kJ mol^{-1}	T interval / ^{o}C	σ_0 / S.cm^{-1}	B / K	T_0 / K	T interval / ^{o}C
MeOAzB/AMPS/MMA	25.6	30 / 80	$2.15 \cdot 10^{-2}$	299	273	80 / 120
NO2AzB/AMPS/MMA	127.0	90 / 130	$5.09 \cdot 10^{-3}$	1095	278	90 / 150
HAzB/AMPS/MMA	61.7	50 / 80	$2.97 \cdot 10^{-3}$	521	253	80 / 150
P(10MeOAzB)-b-PAMPS-b-PMMA [25]	48.0	70 / 120	-	-	-	
P(10-MeOAzB-*co*-AMPS-*co*-MMA) [27]	66.3	70 / 110	-	-	-	

The mechanisms of ionic conductivity through MeOAzB/AMPS/MMA were further investigated by studying its dielectric and cyclic voltammetry response. **Fig. 8(a)** shows the dielectric spectra of this terpolymer, and unveils different relaxations typical of comb-shape liquid crystalline polymers. [57] At low temperatures, -80 / -60^{o}C, we observe a process attributed to the so-called β-relaxation, assigned to rotations of the azobenzene groups around the MeOAzB side-chains. [58, 59] At higher temperatures, the α-relaxation is activated, visible in the 50 / 150^{o}C range in **Fig 8(b)**, and related to the onset of main-chain segmental motions occurring in the vicinity of the glass transition. At the high-temperature end in **Fig. 8(b)**, the δ-relaxation appears, involving the rotation of the MeOAzB side chains along the main polymeric axis. [58]

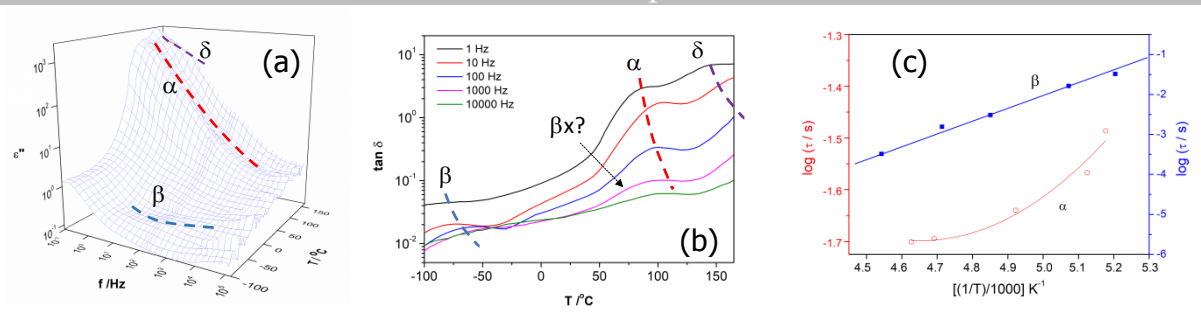

Figure 8. Dielectric response of MeOAzB/AMPS/MMA, highlighting the δ-, α-, βx- and β-relaxations: (a) 3D plot of the temperature and frequency dependence of the loss factor ε"; (b) temperature dependence of tan δ = ε"/ε' at selected frequencies; (c) Arrhenius plots of the relaxation time, τ, corresponding to the α- and β- relaxations.

Based on the corresponding Arrhenius plots in **Fig. 8(c)**, the thermal activation parameters of the β- and α-relaxations of MeOAzB/AMPS/MMA were calculated and are summarised in **Table 5**. The relaxation times (τ) of the β-dielectric relaxation were obtained and fitted to linear Arrhenius behaviour,

$$1/\tau = 1/\tau_0 \exp\left(\frac{E_a}{R}\frac{1}{T}\right) \qquad \text{Eq. 5}$$

where τ_0 is a pre-exponential term. The α-relaxation, which is associated to the glass transition, follows non-Arrhenius temperature dependence that can be described by VFT behaviour,

$$\tau(T)_{max} = \tau_o \exp\left(\frac{B}{T - T_0}\right) \qquad \text{Eq. 6}$$

where τ_0 represents the pre-exponential term, T_0 is the Vogel temperature, which is associated with the cessation of motions of polymeric segments, and *B* is an apparent activation energy. The high E_a values obtained for the β relaxation of MeOAzB/AMPS/MMA in **Table 5** fall within the high range for similar materials. Even though this relaxation is normally attributed to locally activated motions, these values must reflect certain cooperativity of the azobenzene groups in the smectic phase after vitrification at low temperatures.[60]

Table 5. Kinetic parameters of the different dielectric relaxation in MeOAzB/AMPS/MMA, including values obtained for reference comb-shaped poly(methacrylate)s (see structures in **Fig. ESI16**).

Sample	Dielectric relaxations					
	β-relaxation		α-relaxation			
	E_a / kJ mol^{-1}	T interval / °C	-log(t_0/s)	B / K	T_0 / K	T interval / °C
MeOAzB/AMPS/MMA	79.1	-80 / -60	7.8	728	233	65 / 105
P(10MeOAzB)-b-PAMPS-b-PMMA[25]	88.8	-50 / -10	7.6	840	260	40 / 100
P(10-MeOAzB-*co*-AMPS-*co*-MMA)[27]	67.5	-30 / 0	15.6	2741	255	75 / 100
0- MeOAzB/AMPS/MMA[42]	59.1	5 / 30	17.9	1705	300	130 / 165
0.76 MeOAzB/MMA[57]	61.5	-100 / -25	12.9	2574	231	90 / 110
0.22 MeOAzB/MMA [57]	54.6	-110 / -25	7.5	867	305	70 / 120

We note that the activation energy (E_a = 79.1 kJ mol^{-1}) and temperature intervals of the β-relaxation in **Table 5** do not coincide with those calculated for the MeOAzB/AMPS/MMA conductivity measured at low temperatures in **Table 4** (E_a = 25.6 kJ mol^{-1}). Instead, ion conductivity seems to be associated with sub-glass phenomena, such as the so-called βx process related to the AMPS groups, and occurring at intermediate temperatures between the β- and α-relaxations, see **Fig. 8(b)**.[25] We have seen, on the other hand, that the conductivity shown by MeOAzB/AMPS/MMA at high temperatures follow VFT dependence according to Eq. 3, typical of processes involving much higher free volume, and must be activated by the onset of segmental motions in this terpolymer. The thermal parameters of this conductivity process shown in **Table 4**, however, do not match the VFT values calculated for the α-relaxation in **Table 5**. The onset of long-range conductivity in comb-shape liquid crystalline polymers has been instead attributed to the δ- relaxation. [27, 57, 61] This process is normally activated at temperatures above the static glass transition [58], and could be related to the larger mobility of the nematic phase of MeOAzB/AMPS/MMA.

In **Fig. 9** we show the electrochemical response of this terpolymer, in terms of cyclic voltammetry, as an attempt to further investigate local mechanisms of conductivity. The highest occupied molecular orbital energy level, E_{HOMO}, the lowest unoccupied energy level, E_{LUMO}, and the electrochemical band gap, E_g^{el}, were calculated from the following equations,

$$E_{HOMO} = -e[E_{OX/RED} + 4.4] \quad \text{Eq. 7}$$

$$E_{LUMO} = E_{HOMO} + E_g^{el} \quad \text{Eq. 8}$$

where $E_{OX/RED}$ is the first onset oxidation and reduction potential of the terpolymer, and *e* is the electron charge. The external standard potential of ferrocene/ferrocenium ion couple corresponds to the 4.4 eV value in Eq. 7. [62]

From the curves in **Fig. 9(a)** we measured an onset oxidation level of E_{OX} = 0.60 V, and an onset reduction level of E_{RED} = -1.40 V, giving energy levels of E_{HOMO} = -5.40 eV and E_{LUMO} = -3.40 eV. According to these results, we believe that the reduction of MeOAzB/AMPS/MMA starts at the electron transporting segments, which are most likely the N atoms of the azobenzene chromophores and AMPS, while oxidation initiates at the sulfonic terminations, acting as hole transporting sites. According to Eq. 8, the electrochemical band gap calculated from the HOMO/LUMO levels is E_g^{el}~2.00 eV, and the energy band diagram is proposed in **Fig. 9(b)**.

Alternatively, an optical band gap of E_g^{opt}= 3.01 eV can be calculated from the onset of the MeOAzB/AMPS/MMA UV-vis absorption spectrum in **Fig. 5**,

$$E_g^{opt} = h\frac{c}{l_{Edge}} \quad \text{Eq. 9}$$

where *h* is the Planck constant, *c* is the speed of light and l_{Edge} = 412 nm is the terpolymer optical absorbance band edge obtained from the UV-vis spectra.[63] The larger value of E_g^{opt} with respect to E_g^{el} can be due to the reduction and oxidation processes occurring in the fully conjugated system, instead of an isolated electron and hole transport [64], and thus giving an underestimated bandgap from the direct CV measurement. The results highlight the relevance of the molecular aggregates on ion mobility through the condensed phases of MeOAzB/AMPS/MMA, and how phase structure could assist hole conductivity in liquid crystalline electrolytes by reducing the gap between molecular energy levels. [25]

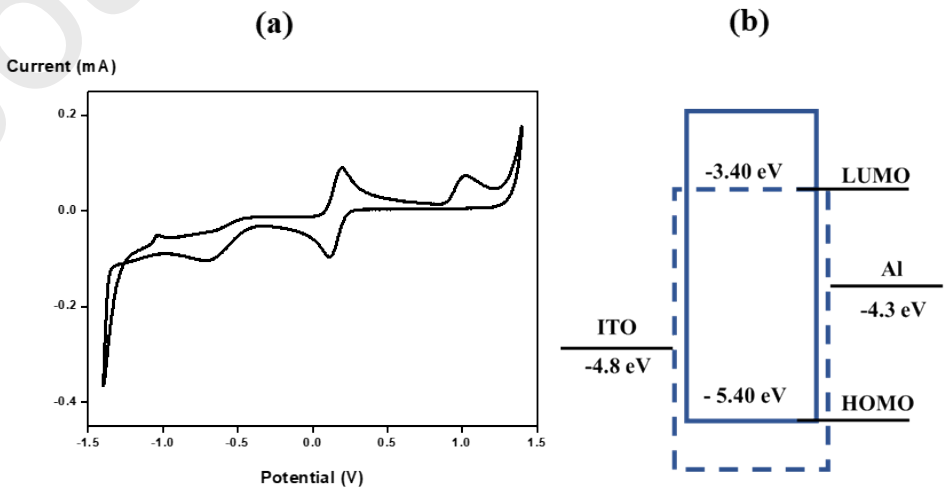

Figure 9. (a) Cyclic voltammogram of the MeOAzB/AMPS/MMA terpolymer film coated on a ITO substrate, in 1 mM $K_4Fe(CN)_6$ in 0.1 M potassium chloride solution; sweep rate 10 $mV \cdot s^{-1}$; (b) energy band diagram of hole transporting segments, ―; electron transporting segments, ---.

Conclusions

We have successfully synthesised a series of poly(methacrylate)-based side-chain liquid crystalline polymers and copolymers, SCLCPs, containing azobenzenes and sulfonic groups as monomeric units, by using one-pot radical polymerisation. *Para*-substitution of the azobenzene with electron-withdrawing and electron-donating groups can tailor phase behaviour and structure, resulting in nematic and smectic mesomorphism (for NO_2- and CH_3O- containing polymers), but also to suppression of liquid crystallinity (for H-substituted azobenzenes). Interestingly, the terpolymer containing methoxy-azobenzene chains, MeOAzB/AMPS/MMA, exhibits high levels of conductivity ($\sim 10^{-2.9}$ $S \cdot cm^{-1}$) in a broad range of temperatures, whilst containing moderate amounts of polarisable sulfonic monomeric units (~ 25%, molar %). We attribute these values to ionic motions in AMPS-rich regions segregated from the mesogenic smectic nanostructure. There are signs of conductivity decoupling from the glass transition of this terpolymer, with electrochemical processes that could be locally activated at the sulfonic terminations of the AMPS chains, which would act as hole transporting sites.

To the best of our knowledge, the conductivity values obtained in this work are within the highest observed under anhydrous conditions for liquid crystalline materials[7], and not far from the results obtained for hydrated perfluorinated benchmark membranes used in commercial fuel cells, such as Nafion (0.1 $S \cdot cm^{-1}$)[65, 66], and confirm the potential of SCLCPs as electrolytes in energy conversion and storage devices. The selective response of these materials to certain UV light, and the reorientation of the smectic layers by external stimuli, such as polarised light, will be the subject of further studies.

Acknowledgements

SMA and NFKA would like to acknowledge Malaysian Ministry of Higher Education, for the grant number 600-IRMI/FRGS 5/3 (374/2019). OKAZ and ARI would like to acknowledge the Sultan Qaboos University, by its support through His Majesty's Trust Fund for Strategic Research (SR/SCI/CHEM/18/01) and Omantel fund (EG/SQU-OT/19/1). TSV acknowledges financial support from the University of Malaya for the RU grant [ST001-2020]. AMF would like to thank the Royal Academy of Engineering, U.K., for the grant NRCP1516/4/61 (Newton Research Collaboration Programme), the University of Aberdeen, for the award of the grant SF10192, the Carnegie Trust for the Universities of Scotland, for the Research Incentive Grant RIG008586, the Royal Society and Specac Ltd., for the Research Grant

RGS\R1\201397, and the Royal Society of Chemistry for the award of a mobility grant (M19-0000). AMF and TSV further acknowledge University Malaya for travelling support.

Data availability

The raw/processed data required to reproduce these findings cannot be shared at this time due to technical or time limitations.

References

1. Cherp A, Jewell J. The three perspectives on energy security: Intellectual history, disciplinary roots and the potential for integration. Current Opinion in Environmental Sustainability 2011 SEP;3(4):202-12.

2. International Energy Agency. Global energy review 2020. Paris: IEA; 2020.

3. Pereira EC, Cuesta A. A personal perspective on the role of electrochemical science and technology in solving the challenges faced by modern societies. J Electroanal Chem 2016 NOV 1;780:355-9.

4. Collings P, Hird M. Introduction to liquid crystals. Chemistry and physics. New York: Taylor & Francis; 1997. .

5. Martinez-Felipe A. Liquid crystal polymers and ionomers for membrane applications. Liquid Crystals 2011 2011;38(11-12):1607-26.

6. Schenning APHJ, Gonzalez-Lemus YC, Shishmanova IK, Broer DJ. Nanoporous membranes based on liquid crystalline polymers. Liquid Crystals 2011 2011;38(11-12):1627-39.

7. Nagao Y. Progress on highly proton-conductive polymer thin films with organized structure and molecularly oriented structure. Science and Technology of Advanced Materials 2020 JAN 1;21(1):79-91.

8. Ichikawa T, Kato T, Ohno H. 3D continuous water nanosheet as a gyroid minimal surface formed by bicontinuous cubic liquid-crystalline zwitterions. J Am Chem Soc 2012 JUL 18;134(28):11354-7.

9. Yabu H, Nagano S, Nagao Y. Core-shell cylinder (CSC) nanotemplates comprising mussel-inspired catechol-containing triblock copolymers for silver nanoparticle arrays and ion conductive channels. Rsc Advances 2018;8(19):10627-32.

10. Cho B. Nanostructured organic electrolytes. RSC Advances 2014 2014;4(1):395-405.

11. Hadjoudis E, Mavridis I. Photochromism and thermochromism of schiff bases in the solid state: Structural aspects. Chem Soc Rev 2004 NOV 30;33(9):579-88.

12. van der Molen SJ, Liljeroth P. Charge transport through molecular switches. Journal of Physics-Condensed Matter 2010 APR 7;22(13):133001.

13. Bleger D, Hecht S. Visible-light-activated molecular switches. Angewandte Chemie-International Edition 2015 SEP 21;54(39):11338-49.

14. Matsuda K, Irie M. Diarylethene as a photo switching unit. Journal of Photochemistry and Photobiology C-Photochemistry Reviews 2004 OCT 15;5(2):169-82.

15. Pfletscher M, Woelper C, Gutmann JS, Mezger M, Giese M. A modular approach towards functional supramolecular aggregates - subtle structural differences inducing liquid crystallinity. Chemical Communications 2016;52(55):8549-52.

16. Wawrzyniak-Adamczewska M, Wierzbowska M. Separate-path electron and hole transport across pi-stacked ferroelectrics for photovoltaic applications. Journal of Physical Chemistry C 2016 APR 14;120(14):7748-56.

17. Concellon A, Blasco E, Pinol M, Oriol L, Diez I, Berges C, Sanchez-Somolinos C, Alcala R. Photoresponsive polymers and block copolymers by molecular recognition based on multiple hydrogen bonds. Journal of Polymer Science Part A-Polymer Chemistry 2014 NOV 15 2014;52(22):3173-84.

18. Concellon A, Blasco E, Martinez-Felipe A, Carlos Martinez J, Sics I, Ezquerra TA, Nogales A, Pinol M, Oriol L. Light-responsive self-assembled materials by supramolecular post-functionalization via hydrogen bonding of amphiphilic block copolymers. Macromolecules 2016 OCT 25;49(20):7825-36.

19. Kreuer K, Portale G. A critical revision of the nano-morphology of proton conducting ionomers and polyelectrolytes for fuel cell applications. Advanced Functional Materials 2013 NOV 20;23(43):5390-7.

20. Kim O, Kim K, Choi UH, Park MJ. Tuning anhydrous proton conduction in single-ion polymers by crystalline ion channels. Nature Communications 2018 NOV 28;9:5029.

21. Liang T, van Kuringen HPC, Mulder DJ, Tan S, Wu Y, Borneman Z, Nijmeijer K, Schenning APHJ. Anisotropic dye adsorption and anhydrous proton conductivity in smectic liquid crystal networks: The role of cross-link density, order, and orientation. Acs Applied Materials & Interfaces 2017 OCT 11;9(40):35218-25.

22. Kumar A, Pisula W, Sieber C, Klapper M, Muellen K. Anhydrous proton conduction in self-assembled and disassembled ionic molecules. Journal of Materials Chemistry A 2018 APR 14;6(14):6074-84.

23. Soberats B, Yoshio M, Ichikawa T, Taguchi S, Ohno H, Kato T. 3D anhydrous proton-transporting nanochannels formed by self-assembly of liquid crystals composed of a sulfobetaine and a sulfonic acid. J Am Chem Soc 2013 OCT 16;135(41):15286-9.

24. Brown AW, Martinez-Felipe A. Ionic conductivity mediated by hydrogen bonding in liquid crystalline 4-n-alkoxybenzoic acids. J Mol Struct 2019 DEC 5;1197:487-96.

25. Mohd Alauddin S, Fadhilah Kamalul Aripin N, Selvi Velayutham T, Martinez-Felipe A. **Liquid crystalline copolymers containing sulfonic and light-responsive groups: From molecular design to conductivity**. Molecules 2020;25(11):2579.

26. Martinez-Felipe A, Lu Z, Henderson PA, Picken SJ, Norder B, Imrie CT, Ribes-Greus A. Synthesis and characterisation of side chain liquid crystal copolymers containing sulfonic acid groups. Polymer 2012 Jun 7;53(13):2604-12.

27. Vanti L, Mohd Alauddin S, Zaton D, Aripin NFK, Giacinti-Baschetti M, Imrie CT, Ribes-Greus A, Martinez-Felipe A. Ionically conducting and photoresponsive liquid crystalline terpolymers: Towards multifunctional polymer electrolytes. European Polymer Journal 2018 December 2018;109:124-32.

28. Yang J, Tan S, Xie W, Luo J, Wang C, Wu Y. Promotion of anhydrous proton conduction by polyvinyl alcohol in liquid crystalline composite membranes containing 1-tetradecyl-3-methylimidazolium hydrogen sulfate. Ionics 2020 APR;26(4):1819-27.

29. Mizumura Y, Hogberg D, Arai K, Sakuda J, Soberats B, Yoshio M, Kato T. Self-assembled liquid-crystalline ion conductors: Odd-even effects of flexible spacers binding a carbonate moiety and an aliphatic rod-like core on phase transition properties and ion conductivities. Bull Chem Soc Jpn 2019 JUL;92(7):1226-33.

30. Concellon A, Hernandez-Ainsa S, Barbera J, Romero P, Luis Serrano J, Marcos M. Proton conductive ionic liquid crystalline poly(ethyleneimine) polymers functionalized with oxadiazole. RSC Adv 2018;8(66):37700-6.

31. Yang X, Tan S, Liang T, Wei B, Wu Y. A unidomain membrane prepared from liquid-crystalline poly(pyridinium 4-styrene sulfonate) for anhydrous proton conduction. J Membr Sci 2017 FEB 1;523:355-60.

32. Kobayashi T, Ichikawa T, Kato T, Ohno H. Development of glassy bicontinuous cubic liquid crystals for solid proton-conductive materials. Adv Mater 2017 JAN 25;29(4):1604429.

33. Concellon A, Liang T, Schenning APHJ, Luis Serrano J, Romero P, Marcos M. Proton-conductive materials formed by coumarin photocrosslinked ionic liquid crystal dendrimers. Journal of Materials Chemistry C 2018 FEB 7;6(5):1000-7.

34. Shibaev VP. Liquid-crystalline polymers: Past, present, and future. Polymer Science Series A 2009 Dec;51(11-12):1131-93.

35. Imrie C, Karasz FE, Attard GS. The effect of molecular-weight on the thermal-properties of polystyrene-based side-chain liquid-crystalline polymers. Journal of Macromolecular Science-Pure and Applied Chemistry 1994;A31(9):1221-32.

36. Craig A, Imrie C. Effect of spacer length on the thermal-properties of side-chain liquid-crystal poly(methacrylate)s. Journal of Materials Chemistry 1994 NOV;4(11):1705-14.

37. Schleeh T, Imrie CT, Rice D, Karasz FE, Attard GS. Ultrastructure studies of polystyrene-based side-chain liquid-crystalline copolymers containing charge-transfer groups. Journal of Polymer Science Part A-Polymer Chemistry 1993 JUN;31(7):1859-69.

38. Aguilar M, Gallardo A, Fernandez M, San Roman J. In situ quantitative H-1 NMR monitoring of monomer consumption: A simple and fast way of estimating reactivity ratios. Macromolecules 2002 MAR 12;35(6):2036-41.

39. Mishra A, Choudhary V. Synthesis, characterizations and thermal behavior of methyl methacrylate and N-(p-carboxyphenyl) methacrylamide/arylamide copolymers. J Appl Polym Sci 2000 OCT 10;78(2):259-67.

40. Talpur M, Oracz P, Kaim A. Study of methyl methacrylate-acrylamide copolymerization system in cyclohexanone in the absence of conventional radical initiator. Polymer 1996 SEP;37(18):4149-54.

41. Martinez-Felipe A, Lu Z, Henderson PA, Picken SJ, Norder B, Imrie CT, Ribes-Greus A. Synthesis and characterisation of side chain liquid crystal copolymers containing sulfonic acid groups. Polymer 2012 JUN 7 2012;53(13):2604-12.

42. Alauddin SM, Aripin NFK, Velayutham TS, Chaganava I, Martinez-Felipe A. The role of conductivity and molecular mobility on the photoanisotropic response of a new azo-

polymer containing sulfonic groups. Journal of Photochemistry and Photobiology A: Chemistry 2020 15 February 2020;389:112268.

43. Scott AJ, Duever TA, Penlidis A. The role of pH, ionic strength and monomer concentration on the terpolymerization of 2-acrylamido-2-methylpropane sulfonic acid, acrylamide and acrylic acid. Polymer 2019 AUG 26;177:214-30.

44. Bouhamed H, Boufi S, Magnin A. Dispersion of alumina suspension using comb-like and diblock copolymers produced by RAFT polymerization of AMPS and MPEG. J Colloid Interface Sci 2007 AUG 15;312(2):279-91.

45. Ferriol M, Gentilhomme A, Cochez M, Oget N, Mieloszynski J. Thermal degradation of poly(methyl methacrylate) (PMMA): Modelling of DTG and TG curves. Polym Degrad Stab 2003 FEB;79(2):271-81.

46. Wang Y, Ma X, Zhang Q, Tian N. Synthesis and properties of gel polymer electrolyte membranes based on novel comb-like methyl methacrylate copolymers. Journal of Membrane Science 2010 Mar 1;349(1-2):279-86.

47. Cook AG, Inkster RT, Martinez-Felipe A, Ribes-Greus A, Hamley IW, Imrie CT. Synthesis and phase behaviour of a homologous series of polymethacrylate-based side-chain liquid crystal polymers. European Polymer Journal 2012 APR 2012;48(4):821-9.

48. Zhu X, Liu J, Liu Y, Chen E. Molecular packing and phase transitions of side-chain liquid crystalline polymethacrylates based on p-methoxyazobenzene. Polymer 2008 Jun 23;49(13-14):3103-10.

49. CRAIG A, IMRIE C. Effect of spacer length on the thermal-properties of side-chain liquid-crystal polymethacrylates .2. synthesis and characterization of the poly[omega-(4'-cyanobiphenyl-4-yloxy)alkyl methacrylate]s. Macromolecules 1995 MAY 8;28(10):3617-24.

50. Imrie CT, Schleeh T, Karasz FE, Attard GS. Dependence of the transitional properties of polystyrene-based side-chain liquid-crystalline polymers on the chemical nature of the mesogenic group. Macromolecules 1993 FEB 1;26(3):539-44.

51. Kumar G, Neckers D. Photochemistry of azobenzene-containing polymers. Chem Rev 1989 DEC;89(8):1915-25.

52. Quick M, Dobryakov AL, Gerecke M, Richter C, Berndt F, Ioffe IN, Granovsky AA, Mahrwald R, Ernsting NP, Kovalenko SA. Photoisomerization dynamics and pathways of trans- and cis-azobenzene in solution from broadband femtosecond spectroscopies and calculations. J Phys Chem B 2014 JUL 24;118(29):8756-71.

53. Merino E, Ribagorda M. Control over molecular motion using the cis-trans photoisomerization of the azo group. Beilstein Journal of Organic Chemistry 2012 JUL 12;8:1071-90.

54. Dyre JC. Some remarks on ac conduction in disordered solids. J Non Cryst Solids 1991 11;135(2–3):219-26.

55. Angell C, Imrie C, Ingram M. From simple electrolyte solutions through polymer electrolytes to superionic rubbers: Some fundamental considerations. Polym Int 1998 SEP;47(1):9-15.

56. Seki S, Susan A, Kaneko T, Tokuda H, Noda A, Watanabe M. Distinct difference in ionic transport behavior in polymer electrolytes depending on the matrix polymers and incorporated salts. J Phys Chem B 2005 MAR 10;109(9):3886-92.

57. Martinez-Felipe A, Santonja-Blasco L, Badia JD, Imrie CT, Ribes-Greus A. Characterization of functionalized side-chain liquid crystal methacrylates containing nonmesogenic units by dielectric spectroscopy. Ind Eng Chem Res 2013 JUL 3 2013;52(26):8722-31.

58. COLOMER F, DUENAS J, RIBELLES J, BARRALESRIENDA J, DEOJEDA J. Side-chain liquid-crystalline poly(n-maleimides) .5. dielectric-relaxation behavior of liquid-crystalline side-chain and amorphous poly(n-maleimides) - a comparative structural study. Macromolecules 1993 JAN 4;26(1):155-66.

59. Nikonorova N, Borisova T, Barmatov E, Pissis P, Diaz-Calleja R. Dielectric relaxation and thermally stimulated discharge currents in liquid-crystalline side-chain polymethacrylates with phenylbenzoate mesogens having tail groups of different length. Macromolecules 2003 JUL 29;36(15):5784-91.

60. SCHONHALS A, WOLFF D, SPRINGER J. Influence of the mesophase structure on the beta-relaxation in comb-like polymethacrylates. Macromolecules 1995 AUG 28;28(18):6254-7.

61. Martinez-Felipe A, Farquharson E, Hashim R, Velayutham TS, Aripin NFK. Glycolipids from natural sources: Dry liquid crystal properties, hydrogen bonding and molecular mobility of palm kernel oil mannosides. Liquid Crystals 2020.

62. Liu G, Zhang B, Chen Y, Zhu C, Zeng L, Chan DS, Neoh K, Chen J, Kang E. Electrical conductivity switching and memory effects in poly(N-vinylcarbazole) derivatives with pendant azobenzene chromophores and terminal electron acceptor moieties. Journal of Materials Chemistry 2011;21(16):6027-33.

63. Chen S, Hwang S, Chen Y. Photoluminescent and electrochemical properties of novel copoly(aryl ether)s with isolated fluorophores. Journal of Polymer Science Part A-Polymer Chemistry 2004 FEB 15;42(4):883-93.

64. Hwang S, Chen Y. Synthesis and electrochemical and optical properties of novel poly(aryl ether)s with isolated carbazole and p-quaterphenyl chromophores. Macromolecules 2001 APR 24;34(9):2981-6.

65. Mauritz KA, Moore RB. State of understanding of nafion. Chemical Reviews 2004 Oct;104(10):4535-85.

66. Martinez-Felipe A, Imrie CT, Ribes-Greus A. Spectroscopic and thermal characterization of the swelling behavior of nafion membranes in mixtures of water and methanol. J Appl Polym Sci 2013 JAN 5 2013;127(1):246-56.

Highlights

New side-chain liquid crystalline terpolymers with anhydrous conductivity: effect of azobenzene substitution on light response and charge transfer.

Sakinah Mohd Alauddin, A. Ramadan Ibrahim, Nurul Fadhilah Kamalul Aripin, Thamil Selvi Velayutham, Osama K. Abou-Zied and Alfonso Martinez-Felipe

- Synthesis of new side-chain liquid crystalline copolymers containing polarisable groups.
- Azobenzene groups confer light-responsive character to the electrolytes.
- Electro-donating and electro-withdrawing groups tailor molecular structure.
- High conductivity values are reached ($10^{-2.9}$ $S \cdot cm^{-1}$) under anhydrous conditions.
- Ion conductivity occurs through nematic and smectic phases, decoupled from the polymer backbone.

New side-chain liquid crystalline terpolymers with anhydrous conductivity: effect of azobenzene substitution on light response and charge transfer.

Sakinah Mohd Alauddin, A. Ramadan Ibrahim, Nurul Fadhilah Kamalul Aripin, Thamil Selvi Velayutham, Osama K. Abou-Zied and Alfonso Martinez-Felipe

CRediT author statement

Sakinah Mohd Alauddin: Resources, Investigation, Formal analysis, Writing.
A. Ramadan Ibrahim: Software, Formal analysis, Investigation.
Nurul Fadhilah Kamalul Aripin: Conceptualization, Methodology, Funding acquisition, Supervision, Writing - Review & Editing.
Thamil Selvi Velayutham: Conceptualization, Funding acquisition, Supervision, Writing - Review & Editing.
Osama K. Abou-Zied: Methodology, Funding acquisition, Supervision, Writing - Review & Editing.
Alfonso Martinez-Felipe: Conceptualization, Methodology,Funding acquisition, Supervision, Writing - Review & Editing.